Supplementary Information

Linear and Nonlinear Optical Properties of Iridium Nanoparticles Grown via Atomic Layer Deposition

Paul Schmitt [1,2,†]**, Pallabi Paul** [1,2,†]**, Weiwei Li** [3,4]**, Zilong Wang** [3,4]**, Christin David** [5]**, Navid Daryakar** [5]**, Kevin Hanemann** [1]**, Nadja Felde** [1]**, Anne-Sophie Munser** [1,2]**, Matthias F. Kling** [3,4,6,7]**, Sven Schröder** [1]**, Andreas Tünnermann** [1,2] **and Adriana Szeghalmi** [1,2,*]

[1] Fraunhofer Institute for Applied Optics and Precision Engineering IOF, Center of Excellence in Photonics, 07745 Jena, Germany
[2] Institute of Applied Physics and Abbe Center of Photonics, Friedrich Schiller University Jena, 07745 Jena, Germany
[3] Physics Department, Ludwig-Maximilians-Universität Munich, 85748 Garching, Germany
[4] Max Planck Institute of Quantum Optics, 85748 Garching, Germany
[5] Institute of Condensed Matter Theory and Optics and Abbe Center of Photonics, Friedrich Schiller University Jena, 07743 Jena, Germany
[6] Stanford Linear Accelerator Center, Stanford University, Menlo Park, CA 94025, USA
[7] Department of Applied Physics, Stanford University, Stanford, CA 94305, USA
[*] Correspondence: adriana.szeghalmi@iof.fraunhofer.de
[†] These authors contributed equally to this work.

Supplementary Information

The film growth of iridium (Ir) deposited on fused silica (FS) via atomic layer deposition (ALD) results in three different growth regions: a linear initial regime, a nonlinear transition regime, and a linear thickness growth regime, as Figure S1a illustrates [1]. The initial regime ($\lesssim$ 200 cycles) represents the initial Ir nucleation and layer formation. In contrast, the thickness growth regime ($\gtrsim$ 250 cycles) corresponds to the Ir ALD thickness growth on an (almost) closed Ir surface. Both regimes continuously merge over the transition regime ($\approx$ 200-250 cycles). In certain regions, the effective Ir layer thickness increases linearly with the number of ALD cycles. For both linear regimes, deposition rates according to growth per cycle (GPC) and nucleation delay (ND) (until the linear growth starts) are calculated.

The Ir surface coverage and layer density increase exponentially saturating with increasing Ir layer thickness. Figure S1b shows the Ir surface coverage on FS substrates analyzed using scanning electron microscopy (SEM) images and the open-source image processing program ImageJ [2]. Initially, the Ir nanoparticles (d $\lesssim$ 2 nm) cover only a small part (f $\lesssim$ 10%) of the substrate surface. The surface coverage increases strongly with increasing effective Ir layer thickness and progressive layer formation. After 150-200 ALD cycles, which corresponds to about 10 nm Ir layer thickness, the coverage amounts to more than 85 %. Approximately, the surface coverage increases exponentially saturating with the Ir layer thickness, as shown in the corresponding fit curve. The relative Ir layer density determined through X-ray reflectometry (XRR) displays a similar trend, as Figure S1b illustrates. Thus, both analysis methods provide consistent and robust values for the so-called volume fill fraction utilized in the effective-medium-approximation (EMA). For modeling using EMA, however, the values determined through SEM were used.
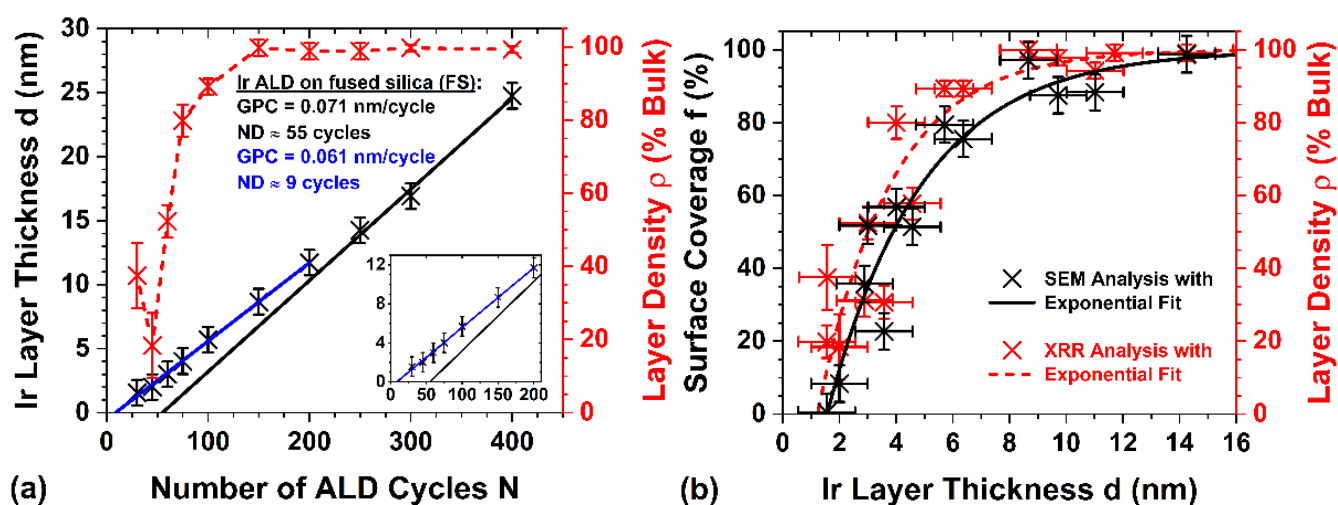
Figure S1. (**a**) Effective Ir layer thickness (black) and layer density (red) of iridium coatings deposited on fused silica (FS) depending on the number of atomic layer deposition (ALD) cycles. In certain regions, the film growth is linearly fitted (black and blue lines) with corresponding growth per cycle (GPC) and nucleation delay (ND) indicated. (**b**) Surface coverage (black) and layer density (red) determined using scanning electron microscopy (SEM) images and X-ray reflectometry (XRR), respectively, with exponentially saturating fit curves (black and red lines) depending on the Ir layer thickness.

The optical constants of the Ir coatings were evaluated using multiple-angle spectroscopic ellipsometry (SE) from 190-980 nm. Therefore, the software package SpetraRay/4 (Sentech Instruments, Berlin, Germany) was used to analyze the ellipsometric amplitude ratio and phase shift, as illustrated in Figure S2. In order to eliminate multiple reflections, the backside of the FS substrate was taped with Magic Tape (3M, Saint Paul, MN, USA), suppressing interfering backside reflections. For all coatings, a three-layer model consisting of an FS substrate, an effective metallic layer using a Drude–Lorentz model with five oscillators, and a surface roughness as an EMA layer, according to Bruggeman, were applied. As determined through XRR, the metallic layer thicknesses were fixed. The EMA layer, consisting of 50 % metal and 50% voids, equaled the XRR surface roughness and was also fixed during the fitting procedure. Figures S2 and S3 show that the ellipsometric parameters were fitted with an excellent agreement for different Ir coatings over the whole spectral and angular range. Hence, this approach relying on XRR and ellipsometry to determine the effective optical constants of metallic islands is auspicious. The effective linear optical properties were subsequently modeled using the Maxwell Garnett approach implemented in the EMA model.
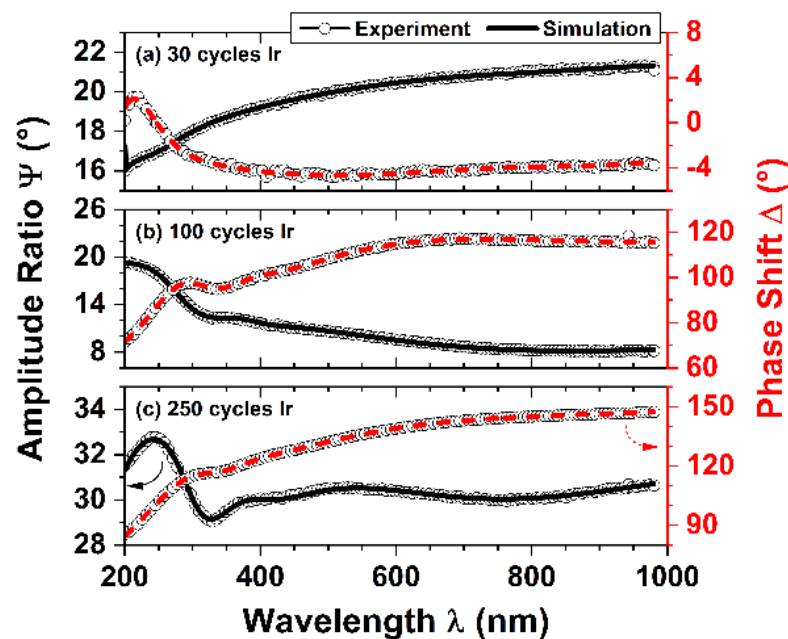
Figure S2. Experimental and fitted ellipsometric amplitude ratio (black) and phase shift (red) of Ir coatings with (**a**) 30, (**b**) 100, and (**c**) 250 ALD cycles. The ellipsometric parameters (exemplary at 70° angle of incidence) were fitted using a Drude–Lorentz model with five oscillators, considering the surface roughness with an effective-medium-approximation (EMA) layer.
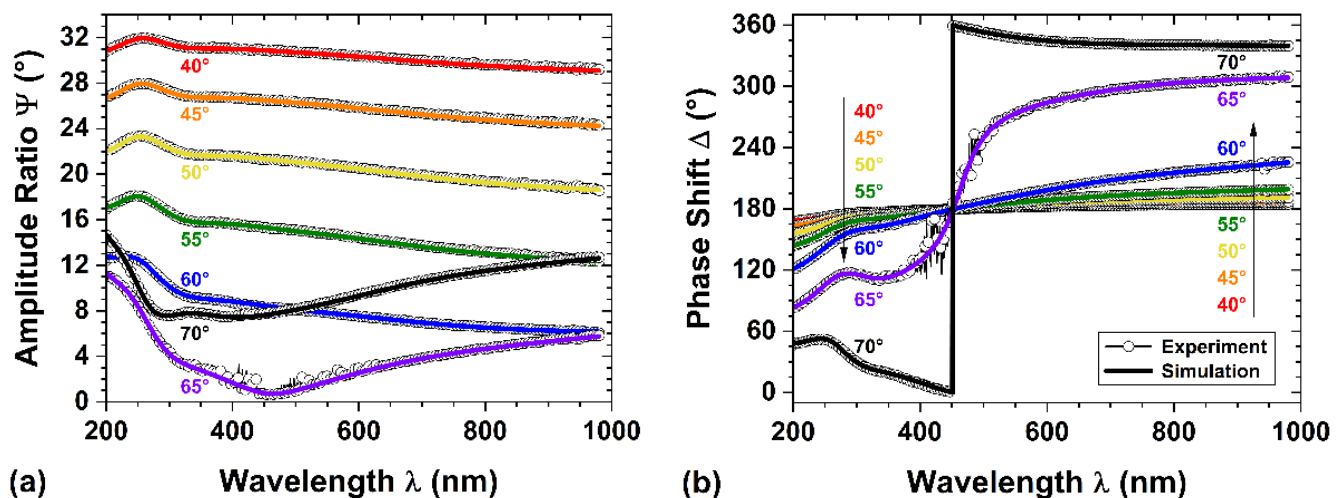

Figure S3. Experimental and fitted data of the ellipsometric (**a**) amplitude ratio and (**b**) phase shift of an Ir coating with 75 ALD cycles. The ellipsometric parameters at different angles of incidence were fitted with excellent agreement over the whole spectral range.

The Ir coating with 100 ALD cycles exhibits the most distinct scattering. Figure S4a shows the angle-resolved scattering (ARS) of selected Ir coatings for the entire forward and backward hemispheres. According to ISO 13696, total scattering (TS) is determined via the ARS integration from θ_S = 2.0-85° in all directions. Figure S4b illustrates the total scattering, consisting of near-angle scattering and far-angle scattering, of Ir coatings depending on their number of ALD cycles. Here, the Ir coating with 100 ALD cycles, which corresponds to about 6 nm effective Ir layer thickness or 70-85 % surface coverage, scatters the most. Thus, the total scattering for a surface with Ir nanoparticles and fully closed Ir layers is significantly smaller. This result is consistent with the optical losses of the Ir coatings from 200-2200 nm wavelength (see Figure 1c in the article). Nevertheless, the total

scattering with TS < 0.08 % is negligible compared to the optical losses of up to 40%, which means that (dissipative) absorption mainly causes the optical losses.
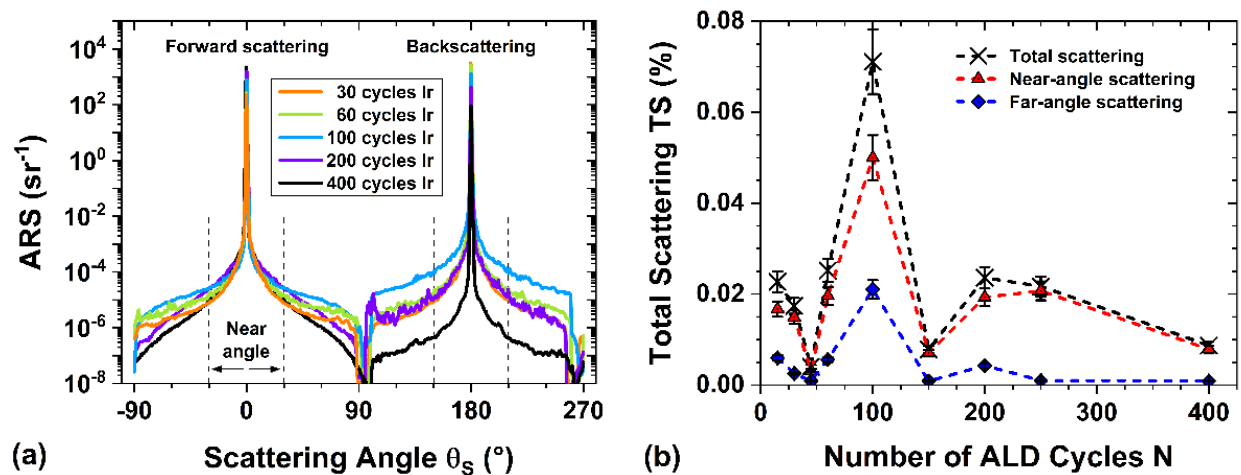

Figure S4. (**a**) Angle-resolved scattering (ARS) of selected Ir coatings whereby the scatterometer measures the entire forward and backward hemisphere. (**b**) Total scattering (TS, black), consisting of near-angle scattering (red) and far-angle scattering (blue), of Ir coatings depending on their number of ALD cycles measured at 405 nm wavelength. Scattering is most pronounced at 100 cycles but overall negligible compared to the dissipative absorption. According to ISO 13696, total scattering is determined through the ARS integration from θ_S = 2.0–85° in all directions; near-normal ARS from 2.0–30°; far-normal ARS from 30–85°.

Figure S5 illustrates bulk and effective susceptibility close to the Mie resonance. Recently, a self-consistent approach was reported to characterize thin films of amorphous composites depending on frequency and thickness [3]. Tables S1 and S2 list the theoretical values of third-order nonlinear susceptibility calculated using the nonlinear Maxwell Garnett theory for selected ultrathin Ir coatings. In Table S1, the nonlinear amplitude was fitted to experimental values; in Table S2, the analytical Miller's rule was used. For comparison, bulk values with a fill fraction of $f = 1$ are given independently from a specific Ir layer thickness.

The third-harmonic wavelength at 233 nm is very close to the Mie resonance of nanosized Ir particles. Thus, the effective Ir susceptibility values are increased by about 5×10^6 compared to the non-resonant case at the fundamental wavelength of 700 nm. Figure S5 illustrates that in some cases, this susceptibility can become the same order as the corresponding bulk values, even for low fill fractions. According to Miller's rule, the analytic case strongly underestimates the nonlinear optical response at finite laser pulses, which can be partially improved by fitting the experimentally determined values. In addition, the influence of the FS nonlinearity on these 1-3 nm Ir NP layers cannot be accounted for; however, it is much stronger than the nonlinearity of the host itself.
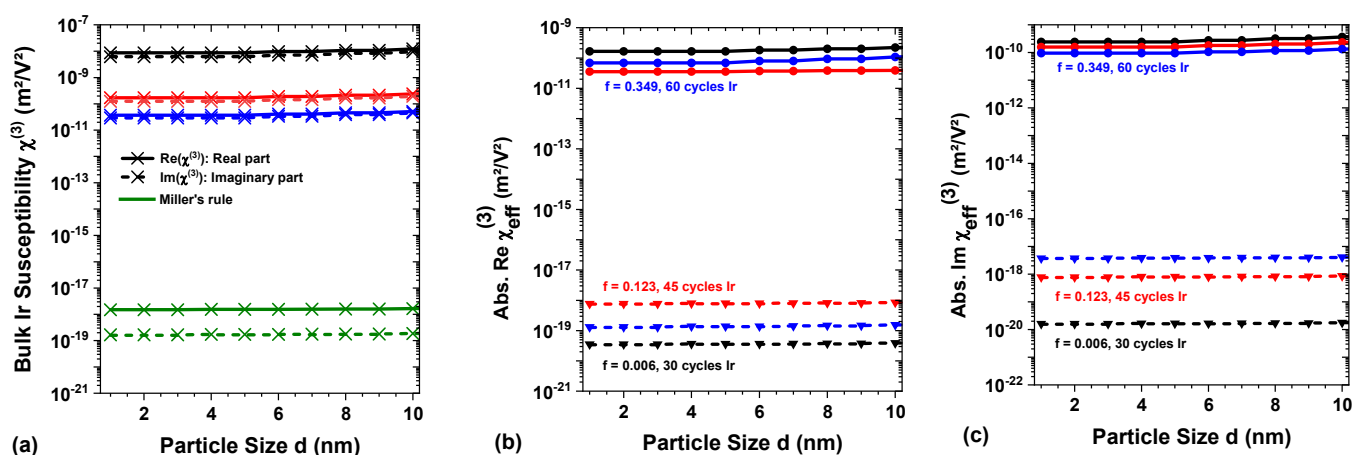
Figure S5. (**a**) Bulk Ir susceptibility with the real (solid) and imaginary (dashed) parts shown separately. Next to fitting the three selected samples, we show the case based on Miller's rule (green curves). (**b**) Real and (**c**) imaginary parts of the effective Ir susceptibility for amorphous Ir coatings depending on particle size, using the experimentally determined fill fraction and layer thickness at 233 nm wavelength. The solid curves originate from the experimentally fitted z-scan data at different ALD cycles, and the dashed curves are derived from Miller's rule.

Finally, we include in Tables S1 and S2 the susceptibilities for coated iridium nanoparticles accounting for an aqueous or hydrocarbon shell possibly forming around the nanoparticles, as discussed in detail in the main article. This shell results in a substantial shift of the Mie resonances for Ir NPs, pushing them closer to the wavelength of the incoming laser field. Thus, the coating brings the susceptibilities closer to the experimentally observed values compared to the standard approach and hints towards the importance of considering a thin film of water or hydrocarbon forming around the Ir NPs.

Table S1. Third-order nonlinear susceptibility calculated from the nonlinear Maxwell Garnett theory with fitting to experimentally obtained values for different samples.

		Pure Iridium Nanoparticles (NP)		Ir NP + CH2-CH-CHO shell	
Number of	Fill	Effective Ir Susceptibility (m²/V²)		Effective Ir Susceptibility (m²/V²)	
ALD Cycles	Fraction	@ 700 nm	@ 233.3 nm	@ 700 nm	@ 233.3 nm
30	0.006	$(3.52 - i3.41)*10^{-17}$	$(1.66 + i2.42)*10^{-10}$	$(1.57 - i1.55)*10^{-17}$	$(5.54 + i3.83)*10^{-12}$
45	0.123	$(2.66 - i2.24)*10^{-17}$	$(3.55 + i5.72)*10^{-11}$	$(1.18 - i1.02)*10^{-17}$	$(2.09 - i3.12)*10^{-12}$
60	0.349	$(7.28 - i3.80)*10^{-17}$	$(-6.93 + i9.46)*10^{-11}$	$(3.42 - i1.75)*10^{-17}$	$(-0.76 + i2.74)*10^{-12}$
		Bulk Ir $\chi^{(3)}$ (m²/V²)			
		$(-2.77 - i0.28)*10^{-12}$	$(-8.68 - i6.16)*10^{-9}$	$(-1.35 - i0.13)*10^{-12}$	$(-2.49 - i0.74)*10^{-10}$
		$(-5.49 - i0.62)*10^{-14}$	$(-1.71 - i1.25)*10^{-10}$	$(-2.67 - i0.30)*10^{-14}$	$(-4.93 - i1.54)*10^{-12}$
		$(-1.21 - i0.19)*10^{-14}$	$(-3.66 - i2.91)*10^{-9}$	$(-5.88 - i0.90)*10^{-15}$	$(-1.07 - i0.38)*10^{-12}$

Table S2. Third-order nonlinear susceptibility as calculated from nonlinear Maxwell-Garnett theory using Miller's rule to obtain an analytic nonlinear amplitude.

		Pure Iridium Nanoparticles (NP)		Ir NP + CH2-CH-CHO shell	
Number of	Fill	Effective Ir Susceptibility (m²/V²)		Effective Ir Susceptibility (m²/V²)	
ALD Cycles	Fraction	@ 700 nm	@ 233.3 nm	@ 700 nm	@ 233.3 nm
30	0.006	$(2.71 + i0.09)*10^{-22}$	$(-1.99 - i2.45)*10^{-17}$	$(2.74 + i0.07)*10^{-22}$	$(-4.47 - i2.60)*10^{-19}$
45	0.123	$(9.65 + i3.47)*10^{-22}$	$(-2.69 - i8.31)*10^{-16}$	$(1.05 + i0.28)*10^{-21}$	$(-9.14 - i11.3)*10^{-18}$
60	0.349	$(6.45 + i5.03)*10^{-21}$	$(-1.37 - i2.52)*10^{-15}$	$(7.56 + i4.15)*10^{-21}$	$(6.47 - i49.21)*10^{-18}$
		Bulk Ir $\chi^{(3)}$ (m²/V²)			
		$(2.99 - i0.06)*10^{-19}$	$(9.85 + i5.88)*10^{-16}$	$(1.04 + i0.02)*10^{-19}$	$(1.96 + i0.41)*10^{-17}$

In the z-scan experiment, the sample's normalized open aperture (OA) result shows a weak positive peak at around Z = 0 (see also Figure 3 in the article), while no OA signal can be found from the bare FS substrate. However, it can be clearly observed that the bare FS substrate contributes significantly to the closed aperture (CA) signal. To eliminate the influence of the substrate, the CA transmittance of the bare FS substrate, as plotted in Figure S6, was also measured under the same experimental condition with the Ir NP samples. The n_2 of bare FS was then obtained by fitting the data with the same formula, which has a value of about -2.11×10^{-20} m^2/W and can serve as a reference. By subtracting this reference value, the actual n_2 values of the Ir NP coatings of 30, 45, and 60 ALD cycles were obtained, as listed in Table 2 in the article.
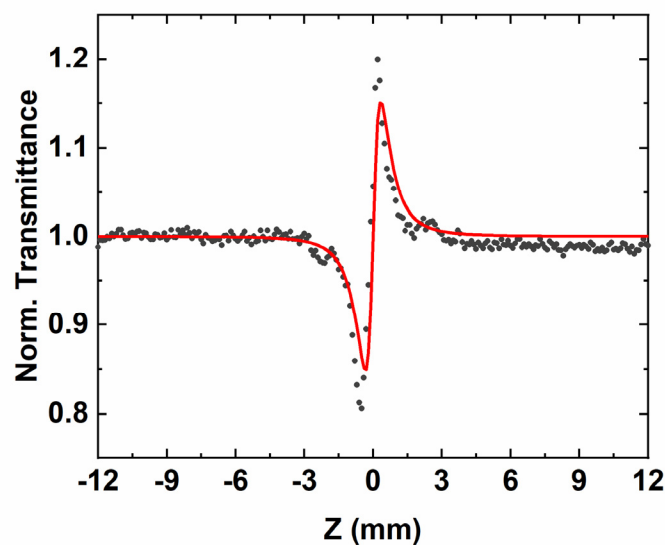

Figure S6. Normalized z-scan closed aperture (CA) transmittance of a bare FS substrate: experimental data (black dots) and the fitted result (solid red curve).

References

(1) Schmitt, P.; Beladiya, V.; Felde, N.; Paul, P.; Otto, F.; Fritz, T.; Tünnermann, A.; Szeghalmi, A. V. Influence of Substrate Materials on Nucleation and Properties of Iridium Thin Films Grown by ALD. *Coatings* **2021**, *11* (2), 173. DOI: 10.3390/coatings11020173.

(2) *ImageJ*. https://imagej.nih.gov/ij/ (accessed 2020-09-10).

(3) Daryakar, N, David. C, Thin Films of Nonlinear Metallic Amorphous Composites, Nanomaterials 2022, 12(19), 3359.

(4) Schmitt, P.; Felde, N.; Döhring, T.; Stollenwerk, M.; Uschmann, I.; Hanemann, K.; Siegler, M.; Klemm, G.; Gratzke, N.; Tünnermann, A.; Schwinde, S.; Schröder, S.; Szeghalmi, A, Optical, structural, and functional properties of highly reflective and stable iridium mirror coatings for infrared applications. Opt. Mater. Express 2021. DOI: 10.1364/OME.447306.